Dynamic Stability of a Microgrid with an Active Load

Nathaniel Bottrell, *Student Member, IEEE,* Milan Prodanovic, *Member, IEEE,* and Timothy C Green, *Senior Member, IEEE*

***Abstract*—Rectifiers and voltage regulators acting as constant power loads form an important part of a microgrid's total load. In simplified form, they present a negative incremental resistance and beyond that, they have control loop dynamics in a similar frequency range to the inverters that may supply a microgrid. Either of these features may lead to a degradation of small-signal damping. It is known that droop control constants need to be chosen with regard to damping, even with simple impedance loads. Actively controlled rectifiers have been modeled in non-linear state-space form, linearized around an operating point, and joined to network and inverter models. Participation analysis of the eigenvalues of the combined system identified that the low-frequency modes are associated with the voltage controller of the active rectifier and the droop-controllers of the inverters. The analysis also reveals that when the active load DC-voltage controller is designed with large gains, the voltage controller of the inverter becomes unstable. This dependency has been verified by observing the response of an experimental microgrid to step changes in power demand. Achieving a well-damped response with a conservative stability margin does not compromise normal active rectifier design, but notice should be taken of the inverter-rectifier interaction identified.**

***Index Terms*—Microgrids; Small-Signal Stability; Inverters; Constant Power Loads; Active Loads; Rectifiers.**

I. Introduction

The presence of distributed generation (DG) in a distribution network creates the possibility of microgrid (MG) formation [1]. If a MG is formed, whether after a line outage or during planned maintenance, there is a need for the DG to respond to changes in load, and share the load such that the DG operate within their limits.

A MG will have to ensure small-signal stability due to small changes to the operating conditions or load perturbations. It is known that, in general, load dynamics interact with generation dynamics and may influence the stability of a network [2]. Therefore, when investigating the stability of a MG, both the generation dynamics and the load dynamics must be considered.

Typically, electrical power in MGs is generated by rotating machines or by power electronics. Rotating machines include synchronous machines and power electronics include voltage or current source inverters. This work only considers MGs with voltage source inverters.

The literature on control approaches that enable the DG to share the load and remain within their operating limits discusses either use of a communications link or use of a droop method. Communication approaches may involve a master-slave link, where the DG outputs are controlled using a dispatch signal [3]. If the master DG unit regulating the grid voltage is not functioning or does not have enough capacity, the MG may not satisfy voltage and frequency limits.

The use of a droop control method has the advantages of not requiring a communication link and allows DG to support MGs irrespective of which sources are available. The droop control method has been widely discussed, for example [4] [5] [6] [7]. However, inverter-interfaced DG operated with droop controllers have relatively complex and dynamic properties.

It is known that in droop controlled MGs, the low-frequency modes (oscillations that are represented by conjugate eigenvalue pairs) are associated with the droop controllers [7]. The low frequency modes are most likely to be poorly damped, and at a risk of instability during operating point or parameter changes. The droop controllers give rise to low frequency modes because of their use of low-pass filters to reject harmonic and negative sequence disturbances from the power measurements. The filtered power measurements are used to determine the frequency references for the AC-voltage controllers of the inverters.

Several strategies have been proposed to increase the damping of the low frequency modes during both steady-state operation and transient behavior. Improvements include adjusting the droop parameters while the MG is functioning by the use of either an energy manager [8] or a grid-impedance estimation strategy [9]. Feed-forward terms have been proposed in [10] and using an inverter to imitate a voltage source with a complex output impedance is proposed in [11]. Using proportional, integral, and derivative controllers within the droop calculation have been proposed in [12] [13] [14] [15].

For simplicity, this work will not consider the enhancements of droop-controllers to improve stability and will only consider the simple droop controller, as presented in [7]. This is so that, the influence of load dynamics within the MG can be more readily observed. One possibility to further simplify the MG model, is to represent the inverters by only their low-frequency dynamics as in [16] (which was extended to larger system sizes in [17]). This modeling technique is valid if the system is not sensitive to the mid-frequency or high-frequency dynamics.

Loads within an electrical network are either passive or ac-

Nathaniel Bottrell and Timothy C Green are with the Department of Electrical and Computer Engineering, Imperial College, London. E-mail: nathaniel.bottrell04@imperial.ac.uk; t.green@imperial.ac.uk. Milan Prodanovic is with IMDEA Energy Institute E-mail: milan.prodanovic@imdea.org;

This work was supported by a Power Networks Research Academy scholarship (http://www.theiet.org/about/scholarships-awards/pnra/). The PNRA is brought together by the IET and funded by four UK power network companies, EA Technology and the EPSRC.

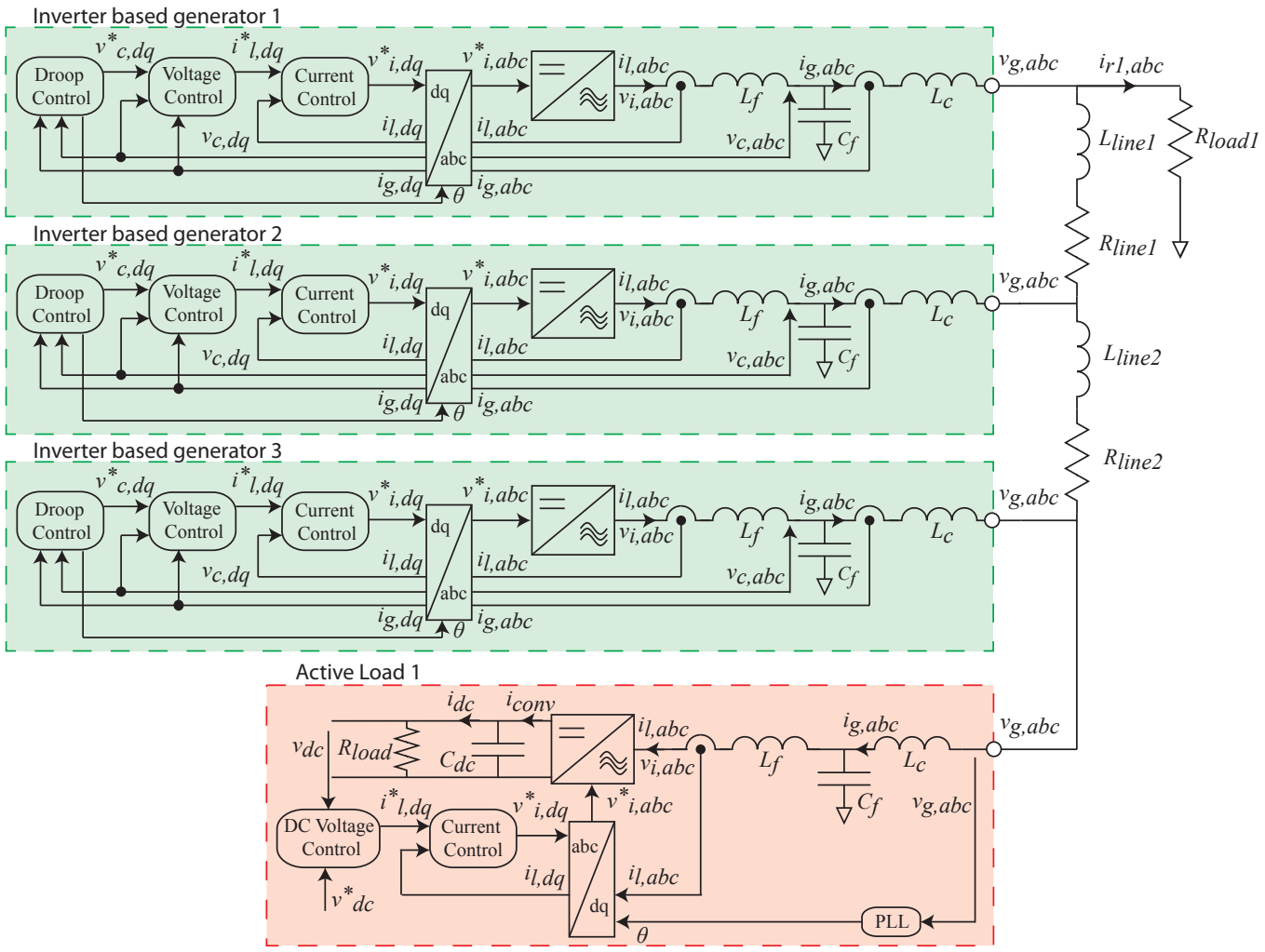

Fig. 1: Comprehensive figure showing all the DG's and loads with corresponding control

tive loads. Passive loads include devices such as incandescent lighting or resistive space heaters and are typically modeled by a resistor or an inductor-resistor network. Active loads include devices such as machine drives, back-to-back converter configurations, and consumer electronics with unity power factor correction. Over a small time period, these devices may be modeled as constant power loads (CPLs). This work considers inverter based generation with active and passive loads.

This work is important since published literature has mostly considered MGs with passive (i.e. impedance) loads, whereas MG implementations are likely to include significant proportions of loads with active front ends. Active front ends are used for providing regulated voltage buses to supply the final use equipment. By regulating the voltage bus, an active load may become a CPL.

Constant impedance loads generally increase damping whereas CPLs tend to decrease damping [18]. To understand how a network responds to different generation technologies, in this case DG, a range of load dynamics must be studied. The results produced from using only passive loads may be misleading, since they might not represent the type of loads connected to a network [19].

CPLs typically destabilize DC MG networks [20] [21] [22] and were shown to destabilize an AC MG in [23], which went on to conclude that CPLs are only stable if paralleled with constant impedance loads. The study used the small-signal representation of an ideal CPL, which exhibits a negative incremental resistance $\left(\Delta i = -\left(\frac{P}{V^2}\right)\Delta v\right)$ but did not consider the dynamics of the bus regulator. Many solutions have been proposed to overcome the problems of CPLs, including the solution discussed in [24] [25].

Large-signal stability of a MG, with various load types, was investigated in [26]. The conclusion from this was that constant PQ loads and impedance loads have no affect on stability but motor loads do. Although this work did not consider small-signal stability, it is important because it demonstrates that CPLs have the possibility of being stable without the need to be paralleled with constant impedance loads (contrary to the assertion in [23]).

Several approaches for determining network stability exist. Power electronic networks can be analyzed using impedance

methods [27]. Impedance methods plot the source and load impedance as a function of frequency. If the source impedance as a function of frequency has a magnitude that is greater than that of the load impedance as a function of frequency, then the system is deemed to be unstable. This method has been used for DC networks and examples in the literature are [28] [29].

Small-signal stability of power systems is often analyzed using eigenvalues of which some examples from literature are [30] [31] [32]. The power system is represented as a state-space equation and the 'A' matrix is used to determine the eigenvalues. One advantage with eigenvalue analysis is the ability to investigate interactions between states.

The approach to be taken follows that of [7] and [33] by using full dynamic models of all elements. This is justified, since the separation of modes into distinct frequency groups (based on controller bandwidths) is still a matter of choice by the equipment designer. Each inverter and load is modeled on a local rotating (dq) reference frame and then the sub-systems are combined onto a common reference frame by the use of rotation functions. The models of inverters will be taken from [7] and models of the active load will be taken from [34]. A laboratory MG with three 10 kVA inverters is used for experimental verification of the analytical results.

Eigenvalue analysis will be used to assess the stability of the system and the sensitivity and damping to change in the gain of the DC-voltage controller of the active load. To determine interactions between the eigenvalues, participation analysis will be performed [35]. Participation analysis allows the investigation of the sensitivity of eigenvalues to the states of the MG and indicates interactions between the dynamics of the inverters and the active load. A full state-space model (rather than a transfer function) allows participation analysis and eigenvalue trace analysis. This allows the influences on poorly damped modes to be explored. The objective for the study reported here is not to analyze the influence of high controller gains, but to examine whether, first, the negative resistance characteristic of active front-end loads have a significant destabilizing effect on MGs and, second, whether there are significant interactions between the dynamics of the inverters and the active loads such that their controllers need coordination or co-design. A comprehensive figure showing all the DG's and loads with corresponding control is shown in Fig. 1.

II. Modeling the Active Load in the MG

A. CPL Model

A theoretical CPL, as shown in Fig. 2, which has the characteristic where $V.I = P$ is modeled. For a CPL, the instantaneous value of impedance is always positive and the incremental impedance is always negative. [24] The negative incremental impedance causes the current to increase when the voltage decreases, and the current to decrease when the voltage increases. It is well known that the negative incremental impedance may cause instabilities [20] [22] [25] [36].

The CPL considered is modeled in series with an inductor and is shown in Fig. 3. The large signal equation is described in (1). Equation (1) is linearized around an operating point and converted to the DQ reference plane which enable the small signal equation in (3) and (4) to be formed. The small signal equation is written as a state-space model in (6).

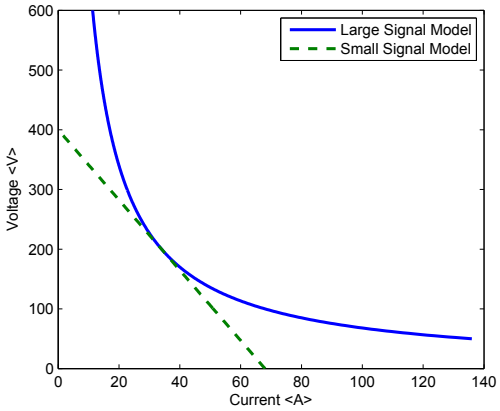

Fig. 2: VI characteristic of a CPL

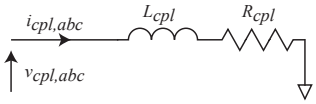

Fig. 3: Circuit of the CPL

Large signal equation of the CPL,

$$\frac{di_{cpl}}{dt} = \frac{-R_{cpl}}{L_{cpl}} i_{cpl} + \frac{1}{L_{cpl}} v_g \tag{1}$$

Where,

$$R_{cpl} = \frac{v_g^2}{P_{cpl}} \tag{2}$$

Small-signal equation of the CPL,

$$\begin{aligned} \frac{d\Delta i_{cplD}}{dt} &= \frac{-R_{cpl}}{L_{cpl}} \Delta i_{cplD} + \omega_0 i_{cplQ} \\ &+ \frac{1}{L_{cpl}} \Delta v_{gD} + I_{cplQ} \Delta \omega_{comm} \end{aligned} \tag{3}$$

$$\begin{aligned} \frac{d\Delta i_{cplQ}}{dt} &= \frac{-R_{cpl}}{L_{cpl}} \Delta i_{cplQ} - \omega_0 i_{cplD} \\ &+ \frac{1}{L_{cpl}} \Delta v_{gQ} + I_{cplD} \Delta \omega_{comm} \end{aligned} \tag{4}$$

Where,

$$R_{cpl} = -\frac{V_{gD}^2}{P_{cpl}} \tag{5}$$

State-space model of the CPL,

$$\begin{aligned} \dot{\left[\Delta i_{cplDQ}\right]} &= A_{cpl} \left[\Delta i_{cplDQ}\right] + B_{cplv} \left[\Delta v_{gDQ}\right] \\ &+ B_{cplw} \left[\Delta \omega_{comm}\right] \end{aligned} \tag{6}$$

Where,

$$A_{cpl} = \begin{bmatrix} \frac{-R_{cpl}}{L_{cpl}} & \omega_0 \\ -\omega_0 & \frac{-R_{cpl}}{L_{cpl}} \end{bmatrix}, B_{cplv} = \begin{bmatrix} \frac{1}{L_{cpl}} & 0 \\ 0 & \frac{1}{L_{cpl}} \end{bmatrix}, \tag{7}$$

$$B_{cplw} = \begin{bmatrix} I_{cplQ} \\ I_{cplD} \end{bmatrix} \tag{8}$$

B. Active Load Model

A switch-mode active rectifier is used in this study as an example of an active load supplying a regulated DC bus. The rectifier is modeled using an averaging method over the switching period, as in [37]. The chosen averaging method is based on the method developed by R. D. Middlebrook and S.Cuk, which averages the circuit states [38]. Models can be readily developed by representing the switching elements as equivalent variable-ratio transformers [39].

Averaged models reflect the key dynamics of the system which are below the switching frequency. In general, the models are non-linear but can be linearized around an operating point [40] [41]. With linear state-space representation, frequency domain analysis can be used to study the system stability.

State-space models of rectifiers that have been previously presented have considered connection to a stiff-grid [42] and have not included the dynamics arising from a supply frequency change. Not accounting for frequency change is a safe assumption when the active load is connected to a large grid or a single frequency source. In large networks, one active load will be a small percentage of the total loads and will not have enough of an effect on the network to cause a frequency disturbance. However, in a small MG with droop controllers, a load change from an active load could be a significant percentage of the total load and have a significant effect on the frequency. For this reason, the frequency of the network must be considered in the active load model.

Switch-mode active loads require an AC-side filter to attenuate switching frequency harmonics. The order and design of the filter varies, with higher order filters being more common in high power equipment. In the laboratory MG, the active load used an LCL filter rather than an LC filter. This offers higher attenuation with smaller passive components. However, lightly damped resonances of LC and LCL filters require careful design of the power converter control loops [42] [43].

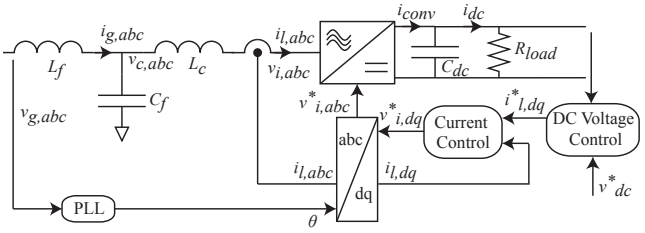

Fig. 4: Active load circuit

An overview of the control system, for the example active load studied here, is shown in Fig. 4. The active load must be synchronized to the network voltage. This is commonly achieved with a phase-lock-loop. In modeling terms, the reference frame of the controller model is made synchronous with the local network voltage. Many different control structures are possible and work in [44] compares different PI current controllers, reviews their advantages, and presents methods of providing active damping. The use of a Linear Quadratic Regulator has also been reported [45]. For this study, a relatively simple structure was adopted which is shown in Fig. 5. All controllers use a PI regulator and the outer DC bus voltage controller forms the reference for an inner current regulator. The inner current regulator is in dq form and regulates the AC-side currents flowing in the inductive element that is between the switching bridge and the AC-side capacitor. No active damping was incorporated but it could be with a relatively simple extension to the model.

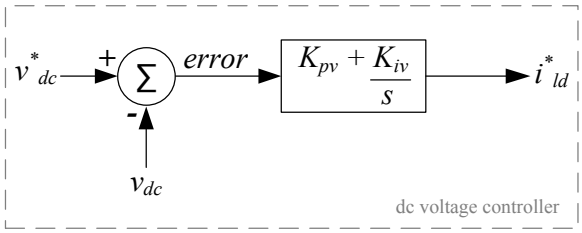

(a) Active load DC voltage controller

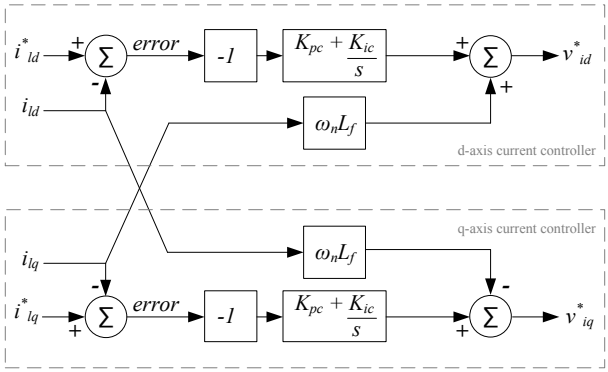

(b) Active load AC current controller

Fig. 5: Active load DC voltage and AC current controller

To design the current controller of the active load, the current controllers that are used within the MG are considered. For the current controllers of the MG inverters, the current is defined as positive when traveling from the switching bridge to the grid connection and (9) (10) apply. [7] [46]

$$v^*_{id} = -\omega_n L_f i_{lq} + K_{pc}\left(i^*_{ld} - i_{ld}\right) + K_{ic}\int\left(i^*_{ld} - i_{ld}\right)dt \quad (9)$$

$$v^*_{iq} = \omega_n L_f i_{ld} + K_{pc}\left(i^*_{lq} - i_{lq}\right) + K_{ic}\int\left(i^*_{lq} - i_{lq}\right)dt \quad (10)$$

However, positive current in the active load is defined as flowing from the grid connection to the switching bridge which is the opposite direction to an inverter. To use the current controllers of the inverter in the active load and compensate, each current measurement was negated and (11) (12) apply. This current controller is shown within Fig. 5 and taken from [34].

$$v^*_{id} = \omega_n L_f i_{lq} - K_{pc}\left(i^*_{ld} - i_{ld}\right) - K_{ic}\int\left(i^*_{ld} - i_{ld}\right)dt \quad (11)$$

$$v_{iq}^{*} = -\omega_n L_f i_{ld} - K_{pc}\left(i_{lq}^{*} - i_{lq}\right) - K_{ic}\int\left(i_{lq}^{*} - i_{lq}\right)dt \quad (12)$$

Transformation of the dq reference frame uses (13). Reference inputs to the controllers are indicated with a superscript asterisk. Upper-case 'D' and 'Q' have been used to denote variables on the common system reference frame of the MG. Lower-case 'd' and 'q' denote variables on the individual reference frame of a particular load or inverter.

The model uses various frequency variables: $\omega, \omega_n, \omega_0$ and ω_{COM}. The variable ω denotes an arbitrary time varying frequency. Nominal system frequency, with a value of $2\pi 50$ in the example here, is denoted by ω_n. The initial frequency at time zero is donated by ω_0 and the common system reference frame frequency is denoted by ω_{COM}.

For simplicity, the model is split into constituent parts. The constituent parts are represented as linear state-space equations and then combined into a single state-space model. This process was presented in [34].

The model of the active load, required for the proposed system study, takes the AC network voltage as its input and returns the resulting AC network current as its output. The model has been divided into various subsystems, such as the DC bus regulator, AC current controller and the filter elements. The modeling of each of these, and their assembly into a complete model of the active load, is described in [34]. The resulting state-space model consists of a state-transition matrix A, matrices for inputs from the AC network voltage B_v, the common system frequency B_ω, and all other inputs B_u. The matrix C_c forms the AC current output, and the matrix C is used to observe other outputs during testing. The matrix D is the feed-forward matrix that directly couples input to output. Finally, a matrix M is used to define the network node, to which the active load model is connected. It also includes a high value resistive path to ground at each node which is there to define the node voltages.

The complete model is shown in (14), and has 10 states, 6 inputs and 3 outputs. All equations are shown with an i subscript to allow for N_i multiple rectifiers to be coupled to a larger circuit model.

$$\begin{aligned}\dot{\left[\Delta x_{RECi}\right]} &= A_{RECi}\left[\Delta x_{RECi}\right] + B_{RECui}\begin{bmatrix}\Delta v_{dc}^{*}\\ \Delta i_{lq}^{*}\end{bmatrix} \\ &+ B_{RECvi}\left[\Delta v_{gDQ}\right] + B_{RECωi}\left[\Delta \omega_{com}\right] \\ &+ B_{RECdci}\left[\Delta\ i_{dc}\right],\end{aligned} \quad (14)$$

$$\begin{aligned}\left[\Delta i_{gDQi}\right] &= C_{RECci}\left[\Delta x_{RECi}\right], \\ \left[\Delta v_{dci}\right] &= C_{RECdci}\left[\Delta x_{RECi}\right].\end{aligned} \quad (15)$$

The states of the rectifier Δx_{RECi} are shown in (16).

$$\Delta x_{RECi} = \left[\Delta\phi_{dci} \mid \ \Delta\gamma_{dqi} \mid \ \Delta i_{ldqi} \quad \Delta v_{cdqi} \quad \Delta i_{gdqi} \mid \ \Delta v_{dci}\right]^{T}. \quad (16)$$

The matrices A_{RECi}, B_{RECui}, B_{RECvi}, $B_{RECωi}$, B_{RECdci}, C_{RECci}, C_{RECdci} form (14) and (15) are defined in equations (17) – (19).

C. Active Load in the MG Model

The active load is connected to node three of the three-node example MG, which is depicted in Fig. 1. By using the method in [34], the matrices of the MG can be systematically built to represent any MG topology. The approach used in [34] can be used on higher dimension MG systems, and could be developed to identify the small-signal stability when integrating DG into the distribution network.

The various subsystems of the example MG will be identified using the subscripts listed in Table I. Each of the subsystems modeled uses the procedure presented in [7]. [34] provides further information about how the components were incorporated into the MG.

One inverter was selected to provide the common system frequency and this is represented in an extra matrix 'C_ω'. The inverter that is the common system frequency has a non-zero 'C_ω' matrix, whereas the other inverters have a zero 'C_ω' matrix. A disturbance component, not shown in Fig. 1, allows a current to be injected or drawn from any node.

Component	Identifying subscript
Inverter	INV
Line	NET
Load	$LOAD$
Active Load	REC
Disturbance	$DIST$

TABLE I: Subscripts for the Components in the MG

The state-space model of the MG that incorporates the active load is summarized by (20), (21), and (22).

III. Identification of Mode Groups

Participation factors can provide a useful insight into what features of a system give rise to a given mode. The participation factor of the ith state and jth eigenvalue is defined as the product of the left eigenvectors (w_{ik}) and right eigenvectors (v_{ki}) [47]:

$$p_{ij} = \frac{|w_{ij}|\,|v_{ji}|}{\sum_{k=1}^{N}\left(|w_{ik}|\,|v_{ki}|\right)} \quad (23)$$

Participation factors are a common tool for accessing the small-signal stability of networks and, as an example, have been used in [7] [48] [49]. The participation matrix is a matrix of all the participation factors. The higher a particular participation factor, the more the state i participates in determining the mode j. Here the highest participation factor for each mode will be used to associate that mode with a particular control subsystem within the MG. The purpose of the participation factor is to produce a state to mode mapping and to identify parameters within the active load and MG that strongly influence the modes of the system.

A. CPL Modeled in the MG

The CPL was connected to node 3 of the MG model and is a substitution for the active load in Fig. 1. Testing with the ideal power load gives an indication as to whether the micro-grid has sufficient damping overall given the negative

$$[T_{dq}] = \sqrt{\frac{2}{3}} \begin{bmatrix} \cos(\omega t + \theta) & \cos\left(\omega t + \theta - \frac{2\pi}{3}\right) & \cos\left(\omega t + \theta + \frac{2\pi}{3}\right) \\ -\sin(\omega t + \theta) & -\sin\left(\omega t + \theta - \frac{3}{2\pi}\right) & -\sin\left(\omega t + \theta + \frac{3}{2\pi}\right) \\ \frac{1}{\sqrt{2}} & \frac{1}{\sqrt{2}} & \frac{1}{\sqrt{2}} \end{bmatrix}. \quad (13)$$

$$A_{RECi} = \begin{bmatrix} 0 & 0 & 0 & B_{V2} \\ B_{C1}C_V & 0 & B_{C2} & B_{C1}D_{V2} \\ B_{LCLu}D_{C1}C_V & B_{LCLu}C_C & A_{LCL} + B_{LCLu}D_{C2} & B_{LCLu}D_{C1}D_{V2} \\ B_{SWu}D_{C1}C_V & B_{SWu}C_C & B_{SW} + B_{LCLu}D_{C2} & A_{SW} + B_{SWu}D_{C1}D_{V2} + B_{SWdc}D_{DCu} \end{bmatrix}_{10\times10}, \quad (17)$$

$$B_{RECui} = \begin{bmatrix} B_{V1} \\ B_{C1}D_{V1} \\ B_{LCLu}D_{C1}D_{V1} \\ B_{SWu}D_{C1}D_{V1} \end{bmatrix}_{10\times2}, \; B_{RECvi} = \begin{bmatrix} 0 \\ 0 \\ B_{LCLv}T_R^{-1} \\ 0 \end{bmatrix}_{10\times2}, \; B_{RECωi} = \begin{bmatrix} 0 \\ 0 \\ B_{LCLω} \\ 0 \end{bmatrix}_{10\times1}, \quad (18)$$

$$B_{RECdci} = \begin{bmatrix} 0 \\ 0 \\ 0 \\ B_{SWdc} \end{bmatrix}_{10\times1}, \; C_{RECci} = \begin{bmatrix} 0 & 0 & \begin{bmatrix} 0 & 0 & T_R \end{bmatrix} & 0 \end{bmatrix}, \; C_{RECdci} = \begin{bmatrix} 0 & 0 & 0 & C_{SW} \end{bmatrix}. \quad (19)$$

$$A_{mg} = \begin{bmatrix} \begin{pmatrix} A_{INV} + B_{INVv}M_{INV}C_{INVc} \\ +B_{INVω}C_{INVω} \end{pmatrix} & B_{INVv}M_{NET}C_{NETc} & B_{INVv}M_{LOAD}C_{LOADc} & B_{RECv}M_{REC}C_{RECc} \\ \begin{pmatrix} B_{NETv}M_{INV}C_{INVc} \\ +B_{NETω}C_{INVω} \end{pmatrix} & A_{NET} + B_{NETv}M_{NET}C_{NETc} & B_{NETv}M_{LOAD}C_{LOADc} & B_{NETv}M_{REC}C_{RECc} \\ \begin{pmatrix} B_{LOADv}M_{INV}C_{INVc} \\ +B_{LOADω}C_{INVω} \end{pmatrix} & B_{LOADv}M_{NET}C_{NETc} & A_{LOAD} + B_{LOADv}M_{LOAD}C_{LOADc} & B_{LOADv}M_{REC}C_{RECc} \\ \begin{pmatrix} B_{RECv}M_{INV}C_{INVc} \\ +B_{RECω}C_{INVω} \end{pmatrix} & B_{RECv}M_{NET}C_{NETc} & B_{RECv}M_{LOAD}C_{LOADc} & \begin{pmatrix} A_{REC} \\ +B_{RECv}M_{REC}C_{RECc} \end{pmatrix} \end{bmatrix} \quad (20)$$

$$B_{mg} = \begin{bmatrix} B_{INVv}M_{DIST}C_{DISTc} & 0 \\ B_{NETv}M_{DIST}C_{DISTc} & 0 \\ B_{LOADv}M_{DIST}C_{DISTc} & 0 \\ B_{RECv}M_{DIST}C_{DISTc} & B_{RECu} \end{bmatrix}, \quad (21)$$

$$C_{mg} = \begin{bmatrix} C_{INV} & 0 & 0 & 0 \\ 0 & 0 & C_{LOAD} & 0 \\ 0 & 0 & 0 & C_{REC} \\ M_{INV}C_{INVc} & M_{NET}C_{NETc} & M_{LOAD}C_{LOADc} & M_{REC}C_{RECc} \end{bmatrix}, \; D_{mg} = \begin{bmatrix} 0 & 0 \\ 0 & 0 \\ 0 & 0 \\ M_{DIST}C_{DISTc} & 0 \end{bmatrix} \quad (22)$$

damping contribution of the CPL. However, it is prudent to follow this with a study with the non-ideal active load. If the eigenvalue plot demonstrates that the MG is unstable for an ideal CPL, it might be reasonable to generalize that a non-ideal CPL would also be unstable. However, there is a limited extent to which this generalization is valid since the non-ideal CPL might have sufficient damping. An ideal CPL is constant power over a large bandwidth whereas the active load (a non-ideal CPL) is only constant power over a limited bandwidth and might appear as a constant current load for a proportion of its bandwidth. This is because the active load consists of two control loops; an inner current controller with a high bandwidth and an outer voltage controller with a low bandwidth.

Fig. 6 shows the eigenvalue plot of the CPL connected to the MG. There are two eigenvalues which are located in on the right-hand side of the imaginary axis. It can be concluded that the MG is unstable when an ideal CPL is connected. The MG without the CPL was shown to be stable in [7].

The two eigenvalues which are unstable have a high participation factor for the coupling inductor state within inverter 3. In this MG, the CPL has caused the inverter which is connected to the node with the CPL to exhibit instabilities.

B. Active Load Modeled in Isolation

Fig. 7 (a) shows the eigenvalue plot of the active load model in isolation, the values for which these were calculated from the A-matrix of the active load. The group of modes labeled

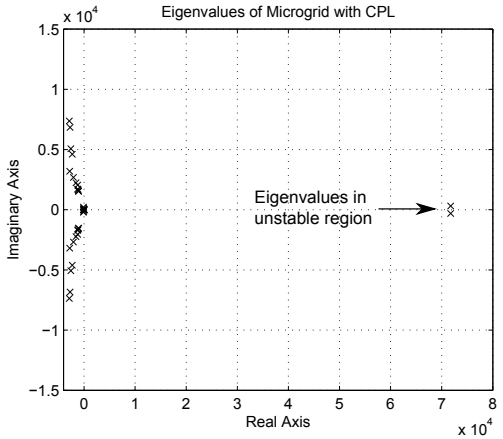

Fig. 6: Eigenvalues of the CPL in the MG model

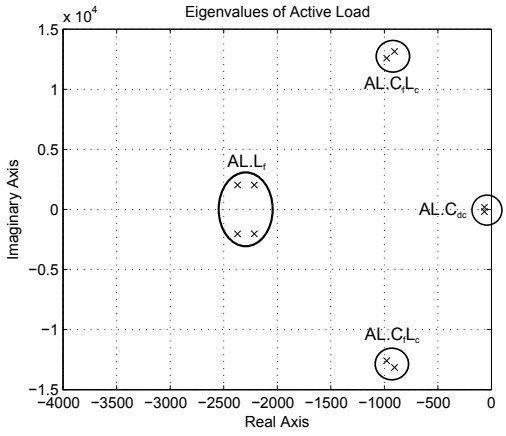

(a) Active load in isolation

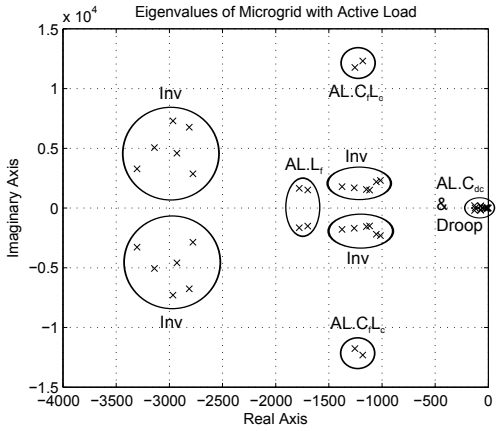

(b) Active load in the MG

Fig. 7: Eigenvalues of the active load and active load in the MG

$AL.C_{dc}$ in Fig. 7 (a), all have high participation factors for the states of the DC-side capacitor and the integrator of the DC bus-voltage regulator. The group labeled $AL.C_fL_c$ are associated with the voltage of the AC-side capacitor C_f and the inductor L_c. The group labeled $AL.L_f$ are associated with the integrator of the current controller and AC-side inductor L_f.

C. Active Load Modeled in the MG

Fig. 7 (b) shown that when the eigenvalues of the complete system (the active load within a MG) are considered, two further mode groups are evident. Groups labeled INV are similar to those found in [7] and are associated with the LCL filter, voltage controller and current controllers of the three inverters. In the group labeled $AL.C_{dc}\&DROOP$, the low frequency modes associated with the active load's DC bus regulator, have been supplemented by the modes associated with the droop controllers of the inverters and so many more eigenvalues are present. A question that arises is whether the modes within the group labeled $AL.C_{dc}\&DROOP$ are two independent subgroups or whether the modes are jointly influenced by the design of the inverters and the active loads.

By observing how the groups associated with the active load change from Fig. 7 (a) to Fig. 7 (b), an understanding of the effect of the MG on the rectifier can be obtained. All three groups appear to be in similar locations on Fig. 7 (a) and Fig. 7 (b), but closer inspection reveals that the groups labeled $AL.L_f$ and $AL.C_f.L_c$ have changed slightly. As already discussed, the groups labeled $AL.L_f$ and $AL.C_f.L_c$ in Fig. 7 are those associated with the LCL filter and the current controllers of the active load. The group labeled $AL.L_f$ has become better damped (with the real part of the eigenvalue changing from approximately $-1,750$ to $-2,300$) and the group labeled $AL.C_f.L_c$ has become slightly less well damped (real part moving from $-1,000$ to $-1,200$).

IV. Identification of Modes Showing Load-Inverter Coupling

Participation analysis not only reveals the states which dominate in formation of the model, but can also reveal second and subsequent influences.

Fig. 8 is a plot of the participation factors of the eigenvalues for the active load states only and reveals the coupling between the active load and the inverters. In Fig. 8 more than one state has been selected for analysis and the participation factors shown on the z-axis are a sum of the participation factors for each state. The x-axis and the y-axis are the real and imaginary axes of the eigenvalue plot. Eigenvalues that have higher participation of the active load states have a longer stem on the x-y-z plot.

It is observed, from Fig. 8 that there is a weak coupling between the active load and the eigenvalues in groups 4 and 5, which are principally associated with the inverters. No coupling is observed in group 1 between the eigenvalues of the active load and the eigenvalues of the inverters.

The conclusion from the participation analysis, is that the droop controllers of the inverters and the controllers of the active load are largely independent (at least for this example), and can be designed on that assumption. The participation analysis indicates a weak coupling between the active load and the inverter voltage and current controllers. In order to ensure that the indicated modes are stable, there needs to be it would be prudent to have an element of co-design or, at the least, design rules should be agreed that allow the two

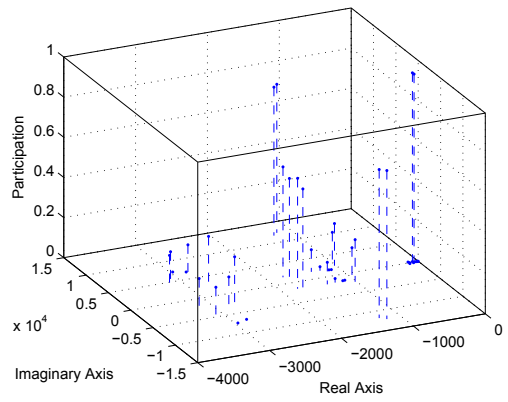

Fig. 8: Participation analysis of the active load in the MG

to be designed by independent parties. If this is not done, the addition of an active load with a certain control characteristics could destabilize the network voltage control.

V. MG Eigenvalue Trace

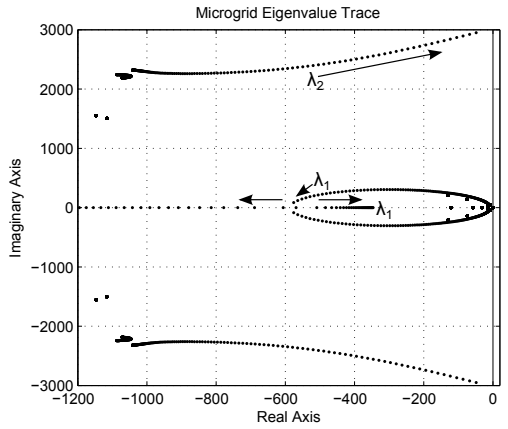

Fig. 9: Low frequency MG eigenvalue trace

It has been shown that coupling exists between the active load and some inverter states (current and voltage controller states) for the example network and with the nominal control gains. Now it is useful to test how damping of the various modes is changed by changes in the load controller parameters.

Fig. 9 shows eigenvalues for the case where the time constant of the DC bus voltage regulator $\left(\tau = \frac{K_{pv}}{K_{iv}}\right)$ was held constant at $\frac{1}{300}$, while the integral gain K_{iv} was varied from 15 to $2,700$ (the value used in the earlier plots was 150). It is seen that two eigenvalues move significantly. The first trace, of λ_1, shows the low frequency modes associated with the DC-voltage controller of the active load, which one would expect to depend on K_{iv}. The second trace, λ_2, is of the modes associated with the AC-voltage controller of the inverters. The second trace shows that high gains in the load controller can lead to very low damping of the inverter voltage controller and a risk of instability.

Fig. 9 also confirms the conclusions drawn from Fig. 8 concerning coupling between the active load and inverters. The active load states do not participate in the low frequency modes of the inverter droop controllers. The evidence for this is that eigenvalues associated with the inverter droop controllers did not move when K_{iv} was changed. The active load states do participate in the mid-frequency modes of the inverters as already seen in Sec. IV, but beyond what was expected. It was not expected that changing the controller gains of the DC-voltage of the active load would have such a significant effect on the mid-frequency modes associated with the voltage controller of the inverter. To investigate this feature further, the participation values were plotted against gain.

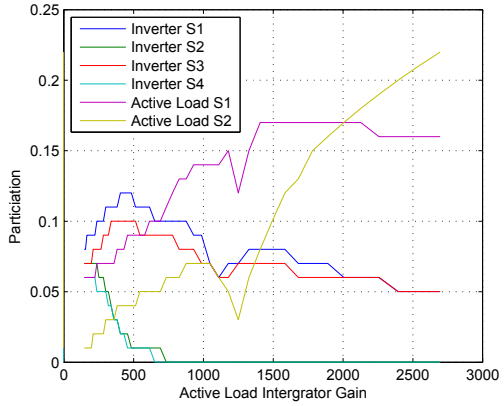

Fig. 10: Participation trace of 4 inverter states and 2 active load states as a function of the active load DC-voltage controller integral gain for the eigenvalue λ_2

State	Description
Inverter S1	Inverter 3 d-axis AC voltage controller state
Inverter S2	Inverter 3 q-axis AC voltage controller state
Inverter S3	Inverter 3 d-axis AC capacitor voltage state
Inverter S4	Inverter 3 q-axis AC capacitor voltage state
Active Load S1	Active Load d-axis AC current state
Active Load S2	Active Load DC capacitor voltage state

TABLE II: Description of the states plotted in Fig. 10

Fig. 10 shows the participations of six states in eigenvalue λ_2 as a function of the gain K_{iv}. Four states from the inverter where chosen because they have the highest participation values at low gain. Two states from the active load are chosen, one state associated with the low-frequency modes and one state associated with the mid-frequency modes. All six states are identified in Table II. It is observed that the participation of the active load states grows rapidly as the gain increases. Also, high K_{iv} causes a further coupling between the DC-voltage controller and AC-current controller of the active load. This informs us that the link between eigenvalues and states may change as the design parameters change. The participation factors only provide information about the system, and its couplings, for a fixed set of design parameters.

The eigenvalue trace in Fig. 9 confirms the results shown in the participation analysis. It can be concluded that the low-frequency modes of the active load do not couple with the low-frequency modes of the inverters. However, there is coupling between the low-frequency modes of the active load and the mid-frequency modes of the inverters when the active load has

high gains in the DC-voltage controller. These couplings must be considered when designing a MG with an active load.

VI. Experimental Results

The example MG of Fig. 1 was available for experimental testing. It was equipped with three 10 kVA inverters operating as droop-controlled sources with a nominal line to line voltage of 381 Vrms (220 Vrms phase to neutral). The active load was provided by another inverter with a further power converter for removing power from the DC bus. Tests at two different gains were conducted to illustrate the results. In each, the power consumption of the active load was stepped from $7,000$ W to $9,000$ W and the transient responses of the load's DC bus voltage, the inverters' output powers and the inverter's d-axis voltage was observed. The gains used, detailed in Table III, correspond to the nominal gains used in the initial analysis and the extreme of the gain range used in Fig. 9. The purpose of the experimental work is to validate the relationship between the active load and the damping of MG modes that was found from the participation analysis.

Test Name	K_{iv}	K_{pv}	$\tau = \frac{K_{pv}}{K_{iv}}$
Low Gain	15	0.05	1/300
Nominal Gain	150	0.5	1/300
High Gain	600	2	1/300
Oscillatory Gain	2700	9	1/300

TABLE III: Gains of DC bus voltage regulator of the active load

A. Transient response with low gain

In this experiment, the low-frequency modes of the MG observed in the time domain are compared to the eigenvalue plot. In Fig. 11 (a) two modes are identified. The mode with a frequency of 10 Hz and a damping factor of 0.208 is associated with the DC voltage controller and DC capacitor of the active load. The mode with a frequency of 4.13 Hz and a damping factor of 0.533 is associated with the droop controllers of the inverters.

Fig. 11 (b) shows that when the load is stepped, the DC voltage oscillates with a frequency of 7 Hz and has a damping factor of 0.377. The envelope of the damping factor is shown by the black long-dash line. The experimental damping factor is slightly less than the model predicts and the frequency observed is in reasonable agreement with the model.

Fig. 11 (c) shows that the three inverters, which have identical droop settings, share the increased power equally when the new steady-state is established. The initial increase in power is all taken by inverter 3, which is electrically closest to the load where the power step occurred. The transient of the power output from inverter 3 has a frequency of 7.14 Hz and has a damping factor of 0.377. The damping factor envelope is shown by the black long-dash line. The observed frequency and damping factor are in reasonable agreement with the model.

Fig. 11 (d) shows the d-axis capacitor voltage of the inverter sources. The power step of the active load change has not

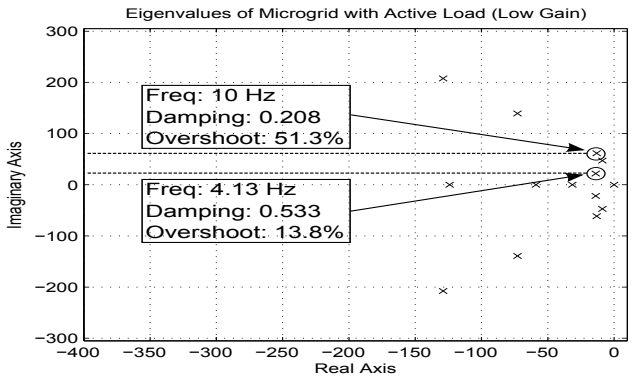

(a) Low frequency modes identified from model

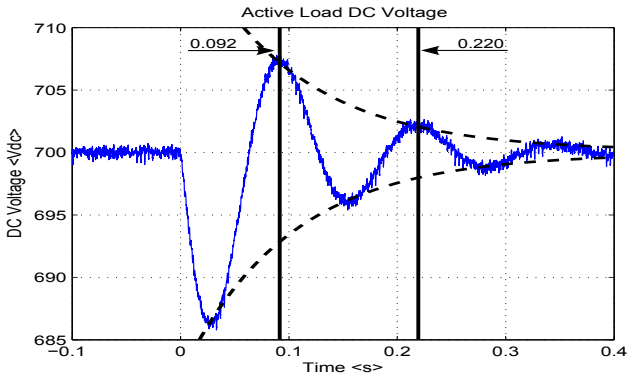

(b) DC voltage of active load

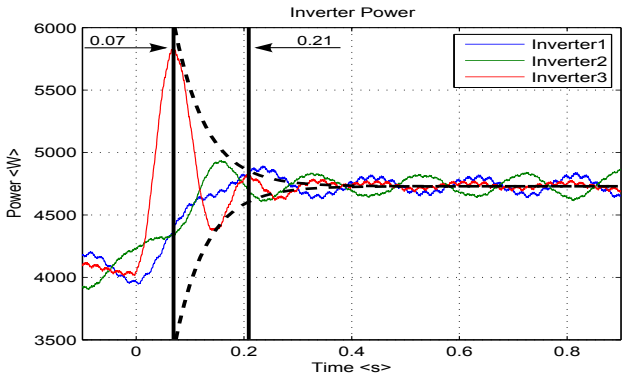

(c) Output power of inverter sources

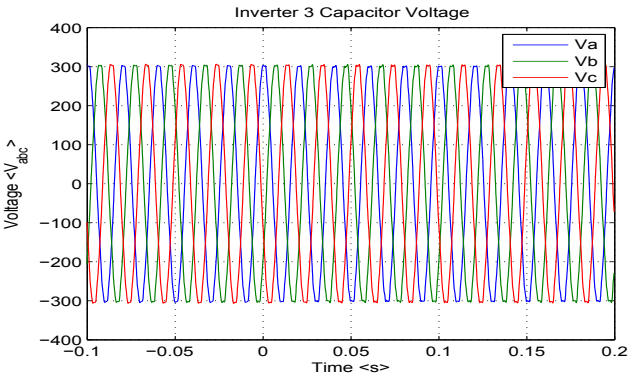

(d) Capacitor voltage of inverter sources

Fig. 11: Experimental results with low gain and active load operating point of 7 kW

caused a noticeable transient in the voltage trace. This figure confirms stable operation of the MG when the active load is perturbed.

B. Transient response with nominal gain

In this experiment, the low-frequency modes of the MG observed in the time domain are compared to the eigenvalue plot. In Fig. 12 (a) two modes are identified. The mode with a frequency of 32 Hz and a damping factor of 0.347 is associated with the DC voltage controller and DC capacitor of the active load. The mode with a frequency of 4.12 Hz and a damping factor of 0.534 is associated with the droop controllers of the inverters.

Fig. 12 (b) shows that when the load is stepped, the DC voltage oscillates with a frequency of 30.3 Hz and has a damping factor of 0.25. The envelope of the damping factor is shown by the black long-dash line. The experimental damping factor is slightly less than the model predicts and the frequency observed is in reasonable agreement with the model.

Fig. 12 (c) shows that the three inverters, which have identical droop settings, share the increased power equally when the new steady-state is established. The initial increase in power is all taken by inverter 3, which is electrically closest to the load where the power step occurred. The transient of the power output from inverter 3 has a frequency of 3.33 Hz and has a damping factor of 0.5. The damping factor envelope is shown by the black long-dash line. The observed frequency and damping factor are in reasonable agreement with the model.

Fig. 12 (d) shows the d-axis capacitor voltage of the inverter sources. The power step of the active load change has not caused a noticeable transient in the voltage trace. This figure confirms stable operation of the MG when the active load is perturbed.

C. Transient response with high gain

In this experiment, the low-frequency modes of the MG observed in the time domain are compared to the eigenvalue plot. In Fig. 13 (a) two modes are identified. The mode with a frequency of 66.2 Hz and a damping factor of 0.208 is associated with the DC voltage controller and DC capacitor of the active load. The mode with a frequency of 4.13 Hz and a damping factor of 0.688 is associated with the droop controllers of the inverters.

Fig. 13 (b) shows that when the load is stepped, the DC voltage oscillates with a frequency of 47.6 Hz and has a damping factor of 0.2244. The envelope of the damping factor is shown by the black long-dash line. The experimental damping factor is slightly less than the model predicts and the frequency observed is in reasonable agreement with the model.

Fig. 13 (c) shows that the three inverters, which have identical droop settings, share the increased power equally when the new steady-state is established. The initial increase in power is all taken by inverter 3, which is electrically closest to the load where the power step occurred. The transient of the power output from inverter 3 has a frequency of 3.17

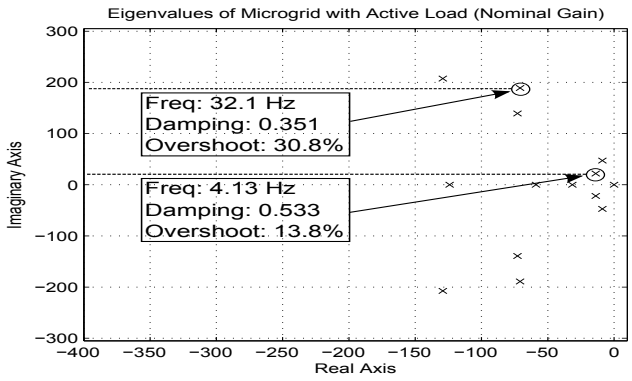

(a) Low frequency modes identified from model

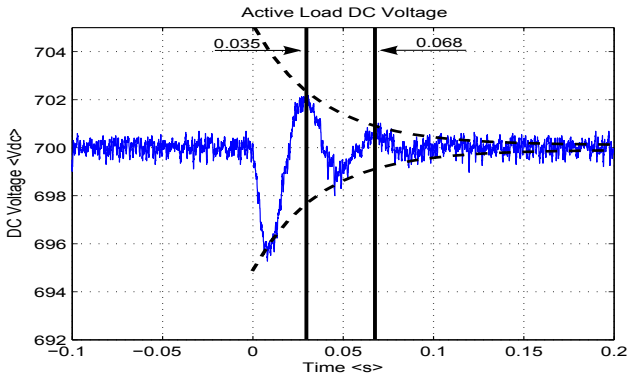

(b) DC voltage of active load

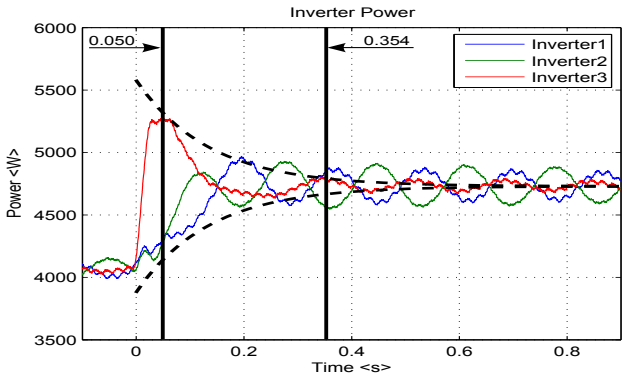

(c) Output power of inverter sources

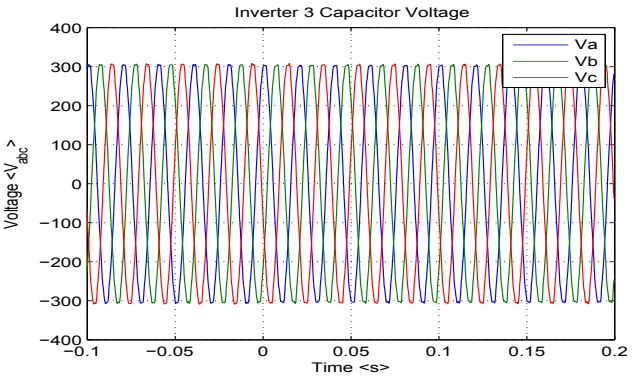

(d) Capacitor voltage of inverter sources

Fig. 12: Experimental results with nominal gain and active load operating point of 7 kW

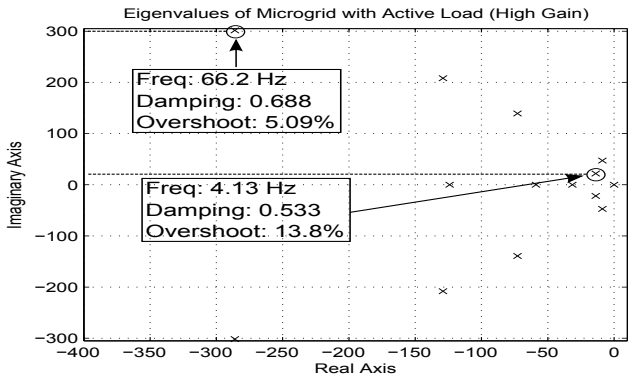

(a) Low frequency modes identified from model

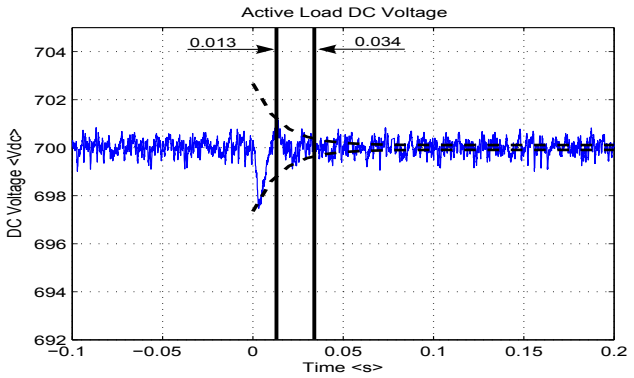

(b) DC voltage of active load

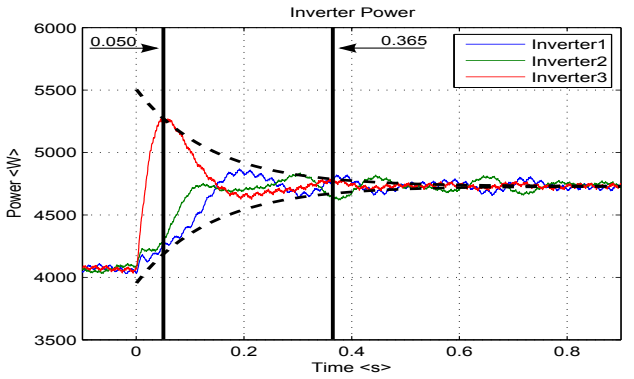

(c) Output power of inverter sources

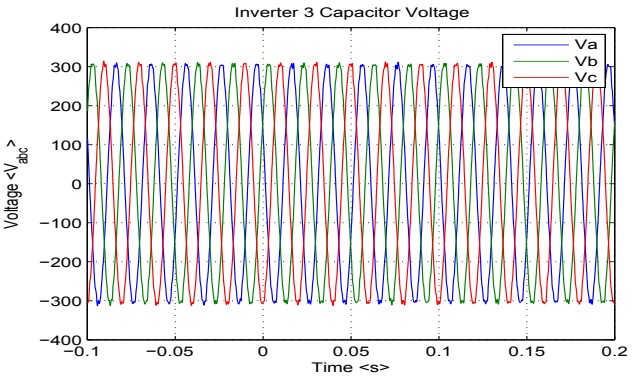

(d) Capacitor voltage of inverter sources

Fig. 13: Experimental results with high gain and active load operating point of 7 kW

Hz and has a damping factor of 0.359. The damping factor envelope is shown by the black long-dash line. The observed frequency and damping factor are in reasonable agreement with the model.

Fig. 13 (d) shows the d-axis capacitor voltage of the inverter sources. The power step of the active load change has not caused a noticeable transient in the voltage trace. This figure confirms stable operation of the MG when the active load is perturbed.

D. Transient response with oscillatory gain

The experiment in Sec. VI-B was repeated for a higher gain in the DC-voltage controller of the active load. The participation analysis of the MG with a high gain in the DC-voltage controller of the active load, showed a link between the active load DC-voltage controller and the inverters' voltage controller. The eigenvalue sweep showed that the eigenvalues, originally associated with the voltage controller of the inverter, becoming unstable and also showed the low frequency eigenvalues remaining stable.

In Fig. 14 (a) two modes are identified. The mode with a frequency of 55.1 Hz and a damping factor of 1 is associated with the DC voltage controller and DC capacitor of the active load. The mode with a frequency of 4.13 Hz and a damping factor of 0.688 is associated with the droop controllers of the inverters.

Fig. 14 (b) shows the DC voltage of the active load. The DC voltage is more oscillatory than at low, nominal or high gain. At the instant of load change, the low frequency transient is not present. However, no obvious transient in this voltage is present when the load is stepped. This absence is explained by the change in position of eigenvalue Fig. 14 (a) which is seen to oscillate with a damping of 1.

Fig. 14 (c) shows the power output of the inverters. The droop controllers have remained stable with a damped response at a frequency of 3.1 Hz. This is a very slight change from the output of the droop controllers in the nominal gain case. The eigenvalue plot in Fig. 9 showed the low frequency modes, associated with the droop controllers, to be unaffected by the gain change.

Fig. 14 (d) shows the capacitor voltage of the inverters. The gains in the inverter have not altered, yet the voltage is non-sinusoidal. Increasing the gain in the DC voltage controller of the load has caused the MG to become unstable. This experimental test confirms the link seen in the eigenvalue trace, where the mid-frequency modes of the inverters move and become coupled with the active load when the gain of the active load DC-voltage controller is increased.

VII. Conclusion

This paper has used a dynamic model of an active load as part of an overall dynamic model of a simple 3-node MG. The active load was modeled as a non-linear state-space model which was joined to a MG, with similar models of droop-controlled inverters and a network, using a common reference frame. The model was linearized about an operating point and participation analysis was used to identify which

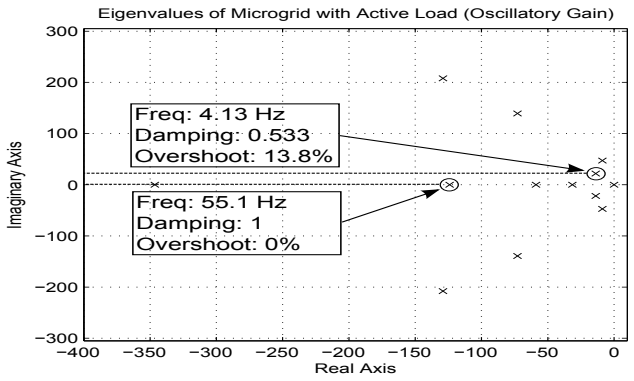

(a) Low frequency modes identified from model

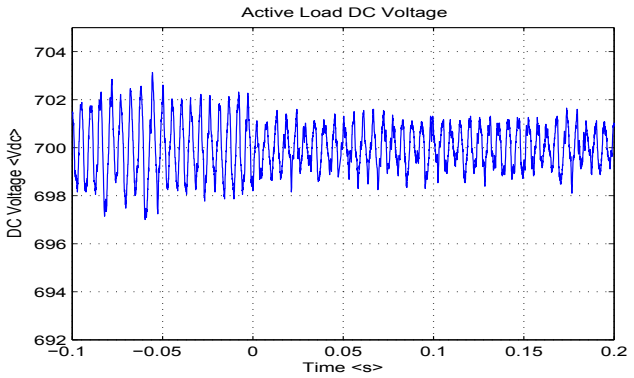

(b) DC voltage of active load

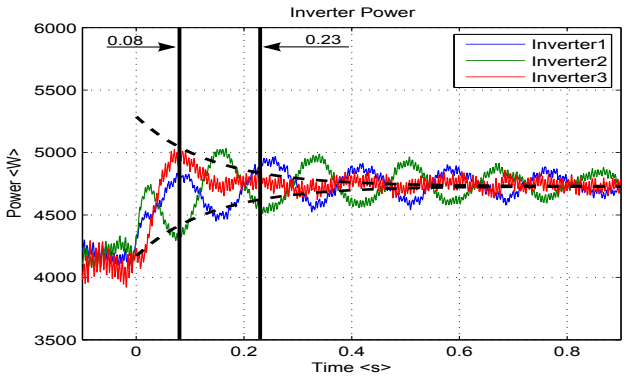

(c) Output power of inverter sources

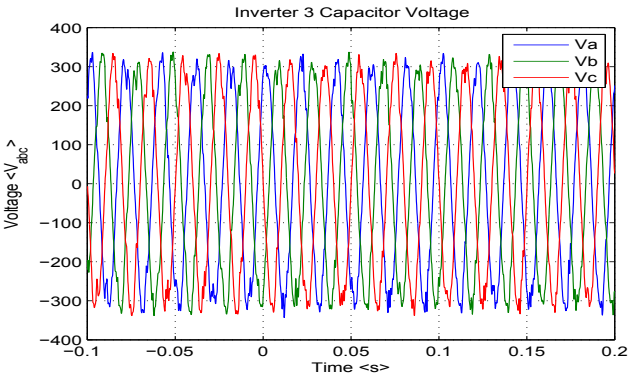

(d) Capacitor Voltage of Inverter Sources

Fig. 14: Experimental results with oscillatory gain

state variables were associated with which eigenvalues. The low frequency eigenvalues, that are associated with either the inverter droop controllers or the DC-voltage controller of the active load, had little interaction. In contrast, a medium-frequency eigenvalue, that was initially associated with the AC-voltage controller of the inverters, became much less damped when the gain of the active load DC-voltage controller was increased.

The system model has been verified against an experimental system with three 10 kVA inverters, one passive load and one active load. Step changes of load were used to excite low-frequency modes and allow observation of frequency and damping factor for two controller gain conditions. Despite initial concerns that the negative resistance property of CPLs would destabilize the power-sharing (droop) controllers, no significant reduction of damping of the low frequency modes was observed for a range of active load voltage control parameters. However, the eigenvalue analysis showed that eigenvalues associated with the DC-voltage controller of the active load moved away from the imaginary axis and the eigenvalues associated with the inverter AC-voltage controller moved towards the imaginary axis as the gain of the rectifier DC-voltage controller was varied. The degradation of damping of this mode was observed in the experiments also.

Although some inverter-rectifier coupling has been identified, it was not in the low-frequency power sharing eigenvalues as anticipated. In the example experimental system, unstable operation did occur for very large gains in the DC voltage loop but these were beyond the gains needed to achieve good steady-state voltage regulation. Therefore it is possible to design the rectifier controller by using conventional frequency domain analysis and independently of the inverter controllers, provided the design is suitably conservative.

ACKNOWLEDGMENT

The authors would like to thank Dr R. Silversides who provided extensive support in setting up the experimental equipment.

REFERENCES

[1] R. H. Lasseter, "Microgrids and Distributed Generation," *Journal of Energy Engineering*, vol. 133, no. 3, pp. 144–149, Sep. 2007.

[2] I. Hiskens and J. Milanovic, "Load Modelling in Studies of Power System Damping," *IEEE Transactions on Power Systems*, vol. 10, no. 4, pp. 1781–1788, Nov. 1995.

[3] B. Bahrani, H. Karimi, and R. Iravani, "Decentralized Control of Parallel Connection of Two Distributed Generation Units," *Industrial Electronics, 2009. IECON '09. 35th Annual Conference of IEEE*, pp. 358 –362, Nov 2009.

[4] M. Chandorkar, D. Divan, and R. Adapa, "Control of Parallel Connected Inverters in Standalone AC Supply Systems," *IEEE Transactions on Industry Applications*, vol. 29, no. 1, pp. 136–143, Jan. 1993.

[5] E. Coelho, P. Cortizo, and P. Garcia, "Small-Signal Stability for Parallel-Connected Inverters in Stand-Alone AC Supply Systems," *Industry Applications, IEEE Transactions on*, vol. 38, no. 2, pp. 533 –542, Mar 2002.

[6] F. Gao and R. Iravani, "A Control Strategy for a Distributed Generation Unit in Grid-Connected and Autonomous Modes of Operation," *Power Delivery, IEEE Transactions on*, vol. 23, no. 2, pp. 850 –859, Apr 2008.

[7] N. Pogaku, M. Prodanovic, and T. C. Green, "Modeling, Analysis and Testing of Autonomous Operation of an Inverter-Based Microgrid," *IEEE Transactions on Power Electronics*, vol. 22, no. 2, pp. 613–625, Mar. 2007.

[8] E. Barklund, N. Pogaku, M. Prodanovic, C. Hernandez-Aramburo, and T. Green, "Energy Management in Autonomous Microgrid Using Stability-Constrained Droop Control of Inverters," *Power Electronics, IEEE Transactions on*, vol. 23, no. 5, pp. 2346 –2352, Sept 2008.

[9] J. Vasquez, J. Guerrero, A. Luna, P. Rodriguez, and R. Teodorescu, "Adaptive Droop Control Applied to Voltage-Source Inverters Operating in Grid-Connected and Islanded Modes," *Industrial Electronics, IEEE Transactions on*, vol. 56, no. 10, pp. 4088 –4096, Oct 2009.

[10] M. Delghavi and A. Yazdani, "An Adaptive Feedforward Compensation for Stability Enhancement in Droop-Controlled Inverter-Based Microgrids," *Power Delivery, IEEE Transactions on*, vol. 26, no. 3, pp. 1764 –1773, Jul 2011.

[11] K. De Brabandere, B. Bolsens, J. Van den Keybus, A. Woyte, J. Driesen, and R. Belmans, "A Voltage and Frequency Droop Control Method for Parallel Inverters," *Power Electronics, IEEE Transactions on*, vol. 22, no. 4, pp. 1107 –1115, Jul 2007.

[12] J. Guerrero, N. Berbel, J. Matas, L. de Vicuna, and J. Miret, "Decentralized Control for Parallel Operation of Distributed Generation Inverters in Microgrids Using Resistive Output Impedance," pp. 5149 –5154, Nov 2006.

[13] F. Katiraei and R. Iravani, "Power Management Strategies for a Microgrid With Multiple Distributed Generation Units," *Power Systems, IEEE Transactions on*, vol. 21, no. 4, pp. 1821 –1831, Nov 2006.

[14] J. Kim, J. Guerrero, P. Rodriguez, R. Teodorescu, and K. Nam, "Mode Adaptive Droop Control With Virtual Output Impedances for an Inverter-Based Flexible AC Microgrid," *Power Electronics, IEEE Transactions on*, vol. 26, no. 3, pp. 689 –701, Mar 2011.

[15] M. Hua, H. Hu, Y. Xing, and J. Guerrero, "Multilayer Control for Inverters in Parallel Operation Without Intercommunications," *Power Electronics, IEEE Transactions on*, vol. 27, no. 8, pp. 3651 –3663, Aug 2012.

[16] M. Marwali, J.-W. Jung, and A. Keyhani, "Stability Analysis of Load Sharing Control for Distributed Generation Systems," *Energy Conversion, IEEE Transactions on*, vol. 22, no. 3, pp. 737–745, Sep. 2007.

[17] S. Iyer, M. Belur, and M. Chandorkar, "A Generalized Computational Method to Determine Stability of a Multi-inverter Microgrid," *Power Electronics, IEEE Transactions on*, vol. 25, no. 9, pp. 2420–2432, Sep. 2010.

[18] M. Kent, W. Schmus, F. McCrackin, and L. Wheeler, "Dynamic Modeling of Loads in Stability Studies," *IEEE Transactions on Power Apparatus and Systems*, vol. PAS-88, no. 5Part-I, pp. 756–763, May 1969.

[19] E. Kyriakides and R. G. Farmer, "Modeling of Damping for Power System Stability Analysis," *Electric Power Components and Systems*, vol. 32, no. 8, pp. 827–837, Aug. 2004.

[20] A. Kwasinski and C. Onwuchekwa, "Dynamic Behavior and Stabilization of DC Microgrids With Instantaneous Constant-Power Loads," *Power Electronics, IEEE Transactions on*, vol. 26, no. 3, pp. 822 –834, Mar 2011.

[21] M. Cespedes, L. Xing, and J. Sun, "Constant-Power Load System Stabilization by Passive Damping," *Power Electronics, IEEE Transactions on*, vol. 26, no. 7, pp. 1832 –1836, Jul 2011.

[22] D. Marx, P. Magne, B. Nahid-Mobarakeh, S. Pierfederici, and B. Davat, "Large Signal Stability Analysis Tools in DC Power Systems With Constant Power Loads and Variable Power Loads; A Review," *Power Electronics, IEEE Transactions on*, vol. 27, no. 4, pp. 1773 –1787, Apr 2012.

[23] D. Ariyasinghe and D. Vilathgamuwa, "Stability Analysis of Microgrids with Constant Power Loads," *Sustainable Energy Technologies, 2008. ICSET 2008. IEEE International Conference on*, pp. 279 –284, Nov. 2008.

[24] A. Emadi, A. Khaligh, C. Rivetta, and G. Williamson, "Constant power loads and negative impedance instability in automotive systems: definition, modeling, stability, and control of power electronic converters and motor drives," *Vehicular Technology, IEEE Transactions on*, vol. 55, no. 4, pp. 1112 –1125, july 2006.

[25] A. Rahimi and A. Emadi, "Active damping in dc/dc power electronic converters: A novel method to overcome the problems of constant power loads," *Industrial Electronics, IEEE Transactions on*, vol. 56, no. 5, pp. 1428 –1439, may 2009.

[26] N. Jayawarna, X. Wu, Y. Zhang, N. Jenkins, and M. Barnes, "Stability of a MicroGrid," *Power Electronics, Machines and Drives, 2006. The 3rd IET International Conference on*, pp. 316–320, Mar. 2006.

[27] X. Feng, Z. Ye, K. Xing, F. Lee, and D. Borojevic, "Individual Load Impedance Specification for a Stable DC Distributed Power System," *Applied Power Electronics Conference and Exposition, 1999. APEC '99. Fourteenth Annual*, vol. 2, pp. 923 –929 vol.2, Mar 1999.

[28] A. Radwan and Y.-R. Mohamed, "Linear active stabilization of converter-dominated dc microgrids," *Smart Grid, IEEE Transactions on*, vol. 3, no. 1, pp. 203 –216, march 2012.

[29] X. Liu, Y. Zhou, W. Zhang, and S. Ma, "Stability criteria for constant power loads with multistage filters," *Vehicular Technology, IEEE Transactions on*, vol. 60, no. 5, pp. 2042 –2049, jun 2011.

[30] Y. Pipelzadeh, B. Chaudhuri, and T. Green, "Wide-area power oscillation damping control through hvdc: A case study on australian equivalent system," in *Power and Energy Society General Meeting, 2010 IEEE*, july 2010, pp. 1–7.

[31] ——, "Coordinated damping control through multiple hvdc systems: A decentralized approach," in *Power and Energy Society General Meeting, 2011 IEEE*, july 2011, pp. 1–8.

[32] W. Du, H. Wang, X. Zhang, and L. Xiao, "Effect of grid-connected solid oxide fuel cell power generation on power systems small-signal stability," *Renewable Power Generation, IET*, vol. 6, no. 1, pp. 24 –37, january 2012.

[33] A. Tabesh and R. Iravani, "Multivariable Dynamic Model and Robust Control of a Voltage-Source Converter for Power System Applications," *Power Delivery, IEEE Transactions on*, vol. 24, no. 1, pp. 462 –471, Jan 2009.

[34] N. Bottrell and T. Green, "Modelling Microgrids with Active Loads," *Thirteenth IEEE Workshop on Control and Modeling for Power Electronics (COMPEL'12)*, pp. 358 –362, Jun 2012.

[35] N. B. P. Kundur and M. Lauby, *Power System Stability and Control*. McGraw-Hill Professional, 1994.

[36] A. Rahimi and A. Emadi, "An analytical investigation of dc/dc power electronic converters with constant power loads in vehicular power systems," *Vehicular Technology, IEEE Transactions on*, vol. 58, no. 6, pp. 2689 –2702, july 2009.

[37] S. Sanders and G. Verghese, "Synthesis of Averaged Circuit Models for Switched Power Converters," *Circuits and Systems, IEEE Transactions on*, vol. 38, no. 8, pp. 905–915, Aug. 1991.

[38] R. Middlebrook and S. Cuk, "A General Unified Approach to Modelling Switching-Converter Power Stages," *International Journal of Electronics*, vol. 42, no. 6, pp. 521–550, Jun. 1977.

[39] C. Rim, D. Hu, and G. Cho, "The Graphical D-Q Transformation of General Power Switching Converters," *Industry Applications Society Annual Meeting, 1988., Conference Record of the 1988 IEEE*, vol. 1, pp. 940–945, Oct. 1988.

[40] S. Sudhoff, S. Glover, P. Lamm, D. Schmucker, and D. Delisle, "Admittance Space Stability Analysis of Power Electronic Systems," *IEEE Transactions on Aerospace and Electronic Systems*, vol. 36, no. 3, pp. 965–973, Jul. 2000.

[41] I. Jadric, D. Borojevic, and M. Jadric, "Modeling and Control of a Synchronous Generator with an Active DC Load," *IEEE Transactions on Power Electronics*, vol. 15, no. 2, pp. 303–311, Mar. 2000.

[42] M. Liserre, F. Blaabjerg, and S. Hansen, "Design and Control of an LCL-Filter-Based Three-Phase Active Rectifier," *Industry Applications, IEEE Transactions on*, vol. 41, no. 5, pp. 1281–1291, Sep. 2005.

[43] V. Blasko and V. Kaura, "A Novel Control to Actively Damp Resonance in Input LC Filter of a Three Phase Voltage Source Converter," *Applied Power Electronics Conference and Exposition, 1996. APEC '96. Conference Proceedings 1996., Eleventh Annual*, vol. 2, pp. 545–551, Mar. 1996.

[44] B.-H. Kwon, J.-H. Youm, and J.-W. Lim, "A Line-Voltage-Sensorless Synchronous Rectifier," *Power Electronics, IEEE Transactions on*, vol. 14, no. 5, pp. 966 –972, Sep. 1999.

[45] S. Alepuz, J. Bordonau, and J. Peracaula, "A Novel Control Approach of Three-Level VSIs Using a LQR-Based Gain-Scheduling Technique," *Power Electronics Specialists Conference, 2000. PESC 00. 2000 IEEE 31st Annual*, vol. 2, pp. 743 –748 vol.2, Jun. 2000.

[46] S. Yang, Q. Lei, F. Peng, and Z. Qian, "A Robust Control Scheme for Grid-Connected Voltage-Source Inverters," *Industrial Electronics, IEEE Transactions on*, vol. 58, no. 1, pp. 202 –212, Jan 2011.

[47] J. B. J. Machowski and J. Bumby, *Power System Dynamics: Stability and Control*. Wiley, 2008.

[48] A. Ostadi, A. Yazdani, and R. Varma, "Modeling and Stability Analysis of a DFIG-Based Wind-Power Generator Interfaced With a Series-Compensated Line," *Power Delivery, IEEE Transactions on*, vol. 24, no. 3, pp. 1504 –1514, Jul 2009.

[49] S. Balathandayuthapani, C. S. Edrington, S. D. Henry, and J. Cao, "Analysis and Control of a Photovoltaic System: Application to a High-Penetration Case Study," *Systems Journal, IEEE*, vol. 6, no. 2, pp. 213 –219, Jun 2012.

Nathaniel Bottrell (S'10) received the M.Eng. degree in Electrical and Electronic Engineering from Imperial College, London, UK., in 2009 and is currently pursuing the Ph.D. degree in Electrical and Electronic Engineering at Imperial College, London, UK.

His research interests include distributed generation, microgrids and the application of power electronics to low-voltage power systems.

Milan Prodanovic (M'01) received the B.Sc. degree in electrical engineering from the University of Belgrade, Belgrade, Serbia, in 1996 and the Ph.D. degree from Imperial College, London, U.K., in 2004.

Milan Prodanovic received a B.Sc. degree in Electrical Engineering from University of Belgrade, Serbia in 1996 and a Ph.D. degree from Imperial College, UK in 2004. From 1997 to 1999 he was engaged with GVS engineering company, Serbia, developing UPS systems. From 1999 until 2010 he was a research associate in the Control and Power Group at Imperial College in London. Currently he is a Senior Researcher and Head of the Electrical Processes Unit at IMDEA Energa Institute, Madrid, Spain. His research interests are in design and control of power electronics converters, RT control systems, micro-grids and distributed generation.

Timothy C. Green (M'89-SM'02) received the B.Sc. degree (first class honours) in electrical engineering from Imperial College, London, U.K., in 1986 and the Ph.D. degree in electrical engineering from Heriot-Watt University, Edinburgh, U.K., in 1990.

He was a Lecturer at Heriot Watt University until 1994 and is now a Professor of Electrical Power Engineering at Imperial College London and Deputy Head of the Control and Power Research Group. His research interest is in using power electronics and control to enhance power quality and power delivery. This covers interfaces and controllers for distributed generation, micro-grids, active distribution networks, FACTS and active power filters. He has an additional line of research in power MEMS and energy scavenging.

Prof. Green is a Chartered Engineer in the U.K. and MIEE.